ON NUMERICAL MODELLING OF SEDIMENT DYNAMICS IN THE EAST-FRISIAN WADDEN SEA

G. Brink-Spalink, E. V. Stanev & J.-O. Wolff

Introduction

Our area of interest, the East Frisian Wadden Sea, is a narrow tidal water body between the Ems river mouth in the West, the Jade Channel in the East, a chain of barrier islands in the North, and the German coast in the South (see Fig. 1). The narrow inlets between the islands basically control the exchange between North Sea water and the water masses that are formed in the backbarrier basins. The dominant physical driving forces in this area are the tides, wind and wind waves. During the flooding phase (rising sea level travelling from West to East along the chain of islands due to the tide) North Sea water enters through the narrow channels with velocities exceeding 1 m/s and being capable of transporting mud as well as sand. During the ebb phase these water masses and suspended sediment flows out to the open sea, again with high velocities through the narrow inlets, and the cycle of ebb and flood starts again.

As has been demonstrated by STANEV *et al*. (2003a,b) there exists a strong asymmetry between the duration of flood and ebb phases. The time it takes from slack water to maximum ebb current is about 1/6 T, T being the tidal period, whereas the time needed from slack water to maximum flood current is 1/3 T. Such a situation is called "ebb-dominated". This asymmetry, which has been clearly identified in observations, numerical modelling and a simple analytical theory by STANEV *et al*. (2003a,b), is thought to influence the net transport of suspended material in the water column through the inlets, thereby changing the grain size distribution and the morphology in the backbarrier basins over longer time periods.

We have investigated the hydrodynamical characteristics of the East Frisian Wadden Sea using a state-of-the-art turbulence model, which was especially developed to represent the most important aspects of Wadden Sea hydrodynamics, i. e. the highly irregular topography and the processes of flooding and drying in the model area.

Before we show and discuss some results from the coupled hydrodynamic-sediment model we will give a brief introduction to the main physical and numerical aspects of the two models, the hydrodynamic part and the sediment part.

The hydrodynamic model (GETM)

In this section we discuss the model set-up and the major characteristics of the model relevant to the physical conditions in the study area. A more detailed description of the numerical model (GETM, General Estuarine Turbulence Model) can be found in BURCHARD & BOLDING (2002). The momentum equations in Cartesian co-ordinates read:

$$\frac{\partial u}{\partial t}+\alpha\left[\frac{\partial\left(u^2\right)}{\partial x}+\frac{\partial(uv)}{\partial y}-fv+\frac{\partial(uw)}{\partial z}\right]=-g\frac{\partial\zeta}{\partial x}+\frac{\partial}{\partial z}\left(A_V\frac{\partial u}{\partial z}\right)+A_H\nabla^2 u \quad (1)$$

$$\frac{\partial v}{\partial t}+\alpha\left[\frac{\partial(uv)}{\partial x}+\frac{\partial\left(v^2\right)}{\partial y}-fu+\frac{\partial(vw)}{\partial z}\right]=-g\frac{\partial\zeta}{\partial y}+\frac{\partial}{\partial z}\left(A_V\frac{\partial v}{\partial z}\right)+A_H\nabla^2 v \quad (2)$$

$$\frac{\partial x}{\partial x}+\frac{\partial v}{\partial y}+\frac{\partial w}{\partial z}=0 \quad (3)$$

Most of the above notations are standard, where u, v and w are the velocity components with respect to the x (east), y (north) and z (upward) direction, respectively, f is the Coriolis parameter, g is the acceleration due to gravity, and ζ is the sea-surface height. The lateral eddy viscosity $A_H(x,y)$ has primarily been introduced to suppress non-physical noise along the open boundaries in a 3-grid-point wide sponge layer, where it changes exponentially from its boundary value of 10^3 m^2s^{-1} to 1/e of this value. In the interior of our model domain, which has a mean depth of less than 10 m, the dissipation is dominated by vertical friction. $A_V(x,y,k,\varepsilon,\alpha)$ is a generalized form of the vertical eddy viscosity coefficient, k the turbulent kinetic energy per unit mass, ε the eddy dissipation rate of kinetic energy due to viscosity, and α a non-dimensional number reducing the influence of some terms in these equations in situations of very thin fluid coverage on the intertidal flats. This process of drying and flooding is incorporated in the hydrodynamical equations through a parameter a which equals unity in regions where a critical water depth D_{crit} is exceeded and which approaches zero when the thickness of the water column $D=H+\zeta$ tends to a minimum value D_{min}:

$$\alpha=\min\left(1,\frac{D-D_{\min}}{D_{crit}-D_{\min}}\right), \quad (4)$$

where the local depth H is a constant over time. In our model simulations the minimum allowable thickness D_{min} of the water column is 2 cm, and the critical thickness is 10 cm. For a water depth greater than 10 cm ($D\geq D_{crit}$ and $\alpha=1$), the full physics are included. In the range between critical and minimal thickness (between 10 and 2 cm) the model physics is gradually switched towards friction domination, i. e. by reducing the effects of horizontal advection and Coriolis acceleration in equations (1) and (2) and varying the vertical eddy viscosity coefficient A_V according to

$$A_V=\nu_t+(1-\alpha)\nu_\alpha \quad (5)$$

where $\nu_\alpha=10^{-1}m^2s^{-2}$ is a constant background viscosity, and the eddy viscosity ν_t is obtained from the relation

$$\nu_t=c_\mu^4\frac{k^2}{\varepsilon}, \quad (6)$$

with $c_\mu=0.56$ (see, e. g., RODI, 1980).

In GETM, the momentum equations (1) and (2) and the continuity equation (3) are supplemented by a pair of equations describing the time evolution of the turbulent kinetic energy k and its dissipation rate ε:

$$\frac{\partial k}{\partial t}-\frac{\partial}{\partial z}\left(\frac{\nu_t}{\sigma_k}\frac{\partial k}{\partial z}\right)=P-\varepsilon \quad (7)$$

$$\frac{\partial\varepsilon}{\partial t}-\frac{\partial}{\partial z}\left(\frac{\nu_t}{\sigma_\varepsilon}\frac{\partial\varepsilon}{\partial z}\right)=\frac{\varepsilon}{k}\left(c_1P-c_2\varepsilon\right), \quad (8)$$

where σ_k and σ_ε are the turbulent Schmidt numbers.

The necessary boundary conditions for this set of differential equations are discussed in detail in BURCHARD & BOLDING (2002) and STANEV *et al*. (2003a).

The model uses terrain-following vertical coordinates. The vertical column extending from the bottom -H(x,y) to the surface $\zeta(x,y,t)$ is divided into N non-intersecting layers, k=1,…,N by introducing internal surfaces z_k, k=1,…,N-1, each depending on the horizontal position (x,y). In the case of σ-coordinates used in the model the thicknesses of the model layers are $h_k=D/N$ for $1\leq k\leq N$.

The vertically staggered grid includes control volumes around pressure grid points. The vertical velocity points are

aboveand below the tracer points, and are also the grid points where the turbulent quantities k, ε and ν_t are computed.

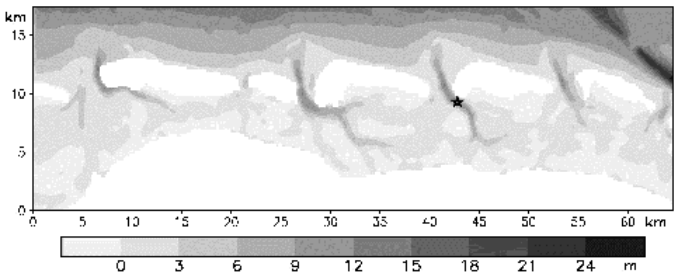

Fig. 1. Bathymetry of the East Frisian Wadden Sea. Shown are depths below mean sea level. The islands are (from left to right) Norderney, Baltrum, Langeoog, Spiekeroog and Wangerooge.

The vertical discretization of our model consists of 10 layers. Because the sea-level height changes continuously during the model integration, and because the thickness of the water column D is a function of sea-level, the vertical discretization changes with time. In our model area the coarsest resolution (in the deepest channels) is ~2 m. When the thickness of water column approaches D_{min} the resolution is ~2 mm The dependence of the layer thicknesses on the local sea-level is quite important, because in large areas of our model domain the water depth becomes similar to the tidal range.

In the horizontal, the grid is a staggered Arakawa-C-grid (ARAKAWA & LAMB, 1977) where the positions of the u-points are west and east, and the positions of the v-points are south and north of the pressure point. A detailed description of the equations and their discretization in time and space is given by BURCHARD & BOLDING (2002).

Advection is treated explicitly with an upstream scheme, whereas vertical diffusion of all variables is treated implicitly, which leads to tri-diagonal linear systems in the vertical. The explicit treatment of advection introduces a time-step constraint through the speed of surface gravity waves which restricts the time step for this mode to 3 s, all internal processes have a time step of 15 s. Our standard experiments have a horizontal resolution of 200 m.

The bathymetry is given by the map shown in Fig. 1. The hydrodynamic model is forced by using sea surface elevation at the northern boundary generated artificially using the tidal components M_2=1.0, S_2=0.3 and K_1=0.1. The resulting tidal signal is shown in Fig. 2.

The sediment transport model

The sediment transport routine is based on the equation:

$$\frac{\partial c}{\partial t}+u\frac{\partial c}{\partial x}+v\frac{\partial c}{\partial y}+w\frac{\partial c}{\partial z}=\frac{\partial}{\partial z}\left(\varepsilon_z\frac{\partial c}{\partial z}\right)+\frac{\partial}{\partial z}(v_s c)+D-E \qquad (9)$$

Here u, v and w are the three velocity components in the x-, y- and z-direction, c is the suspended sediment concentration, A_v is the vertical eddy viscosity coefficient, v_s is the settling velocity of the sediment in suspension, D and E are the deposition rate and erosion rate, respectively.

The settling velocity of sand grains (d>63 µm) is determined by Stokes' formula which is valid for low Reynolds numbers (Re<1):

$$v_s=\frac{g}{18\mu}\frac{\rho-\rho_0}{\rho_0}d^2 \qquad (10)$$

where µ is the kinematic viscosity, ρ and ρ_0 are the densities of the sediment grain and water, respectively, and d is the grain diameter.

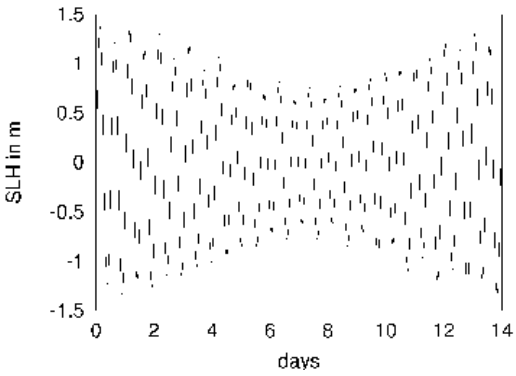

Fig. 2. Artificial tidal signal for the sea level height used as forcing on the northern boundary of the model-area. Shown is a spring-neap-spring-cycle.

The settling velocity of mud particles (d<63 µm) depends on their concentration. Higher concentrations result in a formation of larger aggregates which in turn have a larger settling velocity. Experiments have shown an exponential increase of the settling velocity with the sediment concentration (VAN LEUSSEN, 1988) which is expressed by the formula

$$v_s=k_s c^{m_s} \qquad (11)$$

where c is the suspended sediment concentration of the grain size in question in kgm^{-3} and k_s and m_s are empirical constants. These are chosen to be k_s=0.017 m^{-1} and m_s=1.33 in agreement with the measurements summarized in VAN LEUSSEN (1988).

The deposition rate given by KRONE (1962) is

$$D=c_b\cdot v_s\cdot\left(1-\frac{\tau_0}{\tau_d}\right) \qquad (12)$$

where v_s is the settling velocity, c_b is the suspended sediment concentration near the bottom, τ_b is the shear stress at the bottom and τ_d is the critical shear stress for deposition.

The bottom concentration is extrapolated from the two lowest layers (c_1 and c_2, both located in the middle of the layer) assuming an exponential vertical profile. Thus $c_b=c_1\sqrt{c_1/c_2}$.

The erosion rate is computed using the formula of PARTHENIADES (1984):

$$E=M_e\cdot\left(\frac{\tau_0}{\tau_e}-1\right) \qquad (13)$$

where M_e is an empirical constant and gives the erosion rate at twice the critical shear stress for erosion. α is the fraction of the grain size in question in the bottom sediment and has a value between 0 and 1. The value used for M_e is $3.7\cdot10^{-6}$ $kgm^{-2}s^{-1}$. This is somewhat smaller than the values suggested by other authors (e. g. MEHTA, 1988; PULS & SÜNDERMANN, 1990) ranging between $6\cdot10^{-6}$ and $4\cdot10^{-3}$ $kgm^{-2}s^{-1}$, but showed good results in initial model runs.

The critical shear stress for erosion of sand is computed from BAGNOLD (1966):

$$\tau_e=0.64\rho v_s^{\,2} \qquad (14)$$

where ρ is again the density of water and v_s is the settling velocity. The critical shear stress for erosion of mud is set constant to 0.2 Nm^{-2}. The critical shear stress for deposition is chosen to be equal to that for erosion. That means that either deposition or erosion occurs, and no region of transition exists where none of the two processes is active.

The sediment source at the bottom as a first order approximation is taken to be inexhaustible for sand and mud everywhere. Effects of erosion or deposition on the bathymetry are not considered in our simulations.

Lateral boundary conditions for suspended sediment are taken to be zero for inflowing water. Outflowing water results in a sediment flux of u·c out of the model area, where u is the velocity perpendicular to the boundary and c is the suspended sediment concentration.

In a first run the initial suspended sediment concentration (ssc) was set to zero everywhere. Although the sandy compartments adjusted during one cycle, the finer sediment fractions continuously rose over at least 4 periods. At slack water the sand settles fast enough to be completely deposited, whereas the mud is accumulated in the water column, and an equilibrium is not reached before 4 tidal periods. Thus the suspended sediment concentration field after 4 tidal cycles of a run started with ssc=0 was taken as the initial field for all other runs. This method reduces the adjusting time to one cycle.

The sediment transport routine is not started until half a tidal period has passed to let the hydrodynamics adjust to the forcing. This avoids a non-realistic high erosion rate in some areas.

Results

Fig. 3 shows the time *versus* depth diagram for mud and sand over three tidal cycles around spring tide at a position in the tidal channel of Otzum (Otzumer Balje) just south of the west end of the island of Spiekeroog (indicated by the star in Fig. 1). Sand is transported near the bottom with maximum concentrations when current velocities are highest. It vanishes from the water column during slack water, whereas large amounts of the mud stay in suspension. The maxima of mud concentrations are shifted with respect to the maxima of sand in suspension indicating that mud is still eroded and accumulates in the water column while sand already settles down and is being redeposited. The highest mud concentrations are reached approximately one hour after the highest current velocities.

The response of the sediment dynamics to different wind strengths is presented in Fig. 4. In these model runs the tidal prism is equal for all wind strengths because in all cases the same forcing tide at the northern boundary has been applied. Thus only the effect of the surface wind stress can be seen in these results. The top three graphs show the dynamics of mud, and the bottom row shows the dynamics of sand transport in the Otzumer Balje.

The vertical mean of the concentration of mud and sand in suspension can be seen in the left graphs of Fig. 4 repeating the results already seen in Fig. 3 for the no-wind case. A weak wind of 3 Bft has scarcely any effect on the sediment transport. But for 6 and 9 Bft the concentrations of mud and sand in suspension rise by a factor of approximately 1.3 and 2.5, respectively. Especially for the flood phases the mud and sand concentrations are very high.

Expressed in transport through the Otzumer Balje (middle graphs) this results in a much higher transport of material during strong wind events with higher transport rates during flood. This is most pronounced for the sand transport. Also the tidal asymmetry described in more detail in STANEV *et al*. (2003b) can be seen here: The time interval from maximum flood to maximum ebb current is much smaller than the time interval from maximum ebb to maximum flood current.

Clearly the different transport rates during flood and ebb must result in a net import of material into the tidal basin for windy conditions. This is illustrated in the right graphs of Fig. 4, where the accumulated sediment is plotted. Also the mean over one tidal cycle is plotted to filter out the tidal signal. Whereas for no-wind and low-wind (3 Bft) conditions no net sand transport occurs and mud is even exported from the inlet, both mud and sand are being accumulated when strong winds are active from north-west.

This import of mud during strong wind events was also measured by SANTAMARINA & FLEMMING (2000) for the same tidal inlet. What happens now if the storm event is over? To answer this question, the wind has been switched off after some tidal cycles, and the fate of the mud was investigated. The results are shown in Fig. 5. In the moment of turning off the wind a large amount of the mud in suspension settles down increasing the accumulated mud on the ground of the basin. During the following tides the mud is gradually exported through the inlet as could be assumed from Fig. 4 (top right).

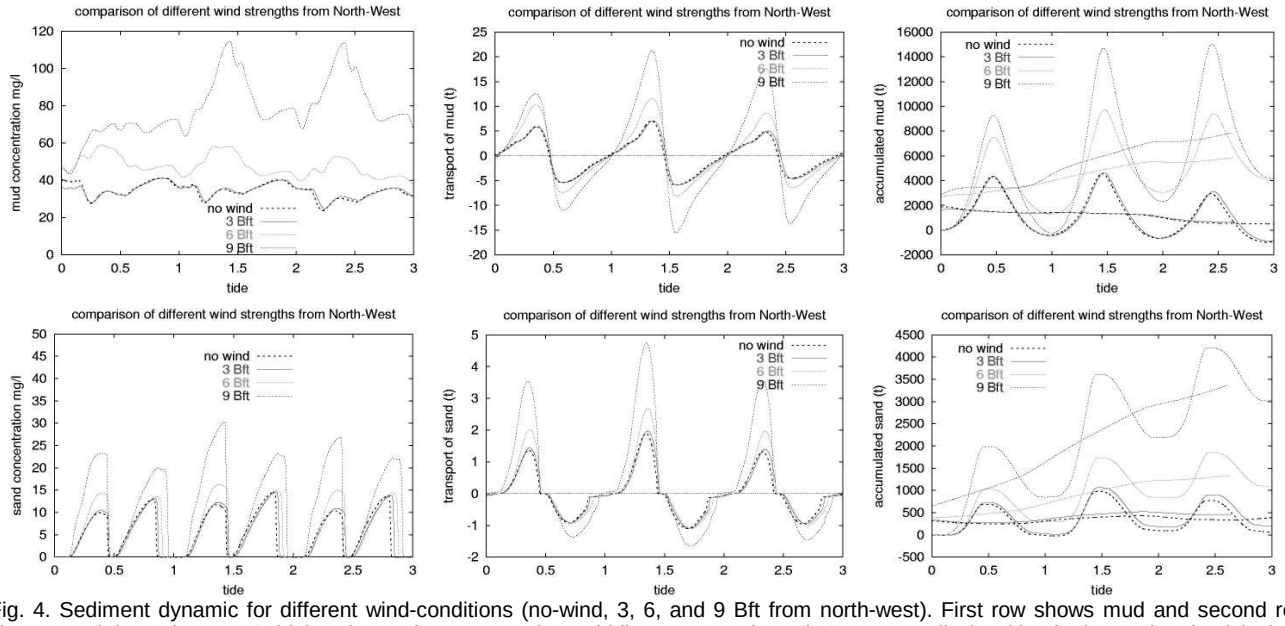

Fig. 4. Sediment dynamic for different wind-conditions (no-wind, 3, 6, and 9 Bft from north-west). First row shows mud and second row shows sand dynamics over 3 tidal cycles. Left: concentration, middle: transport through Otzumer Balje (positive for import into basin), right: accumulated sediment in backbarrier basin.

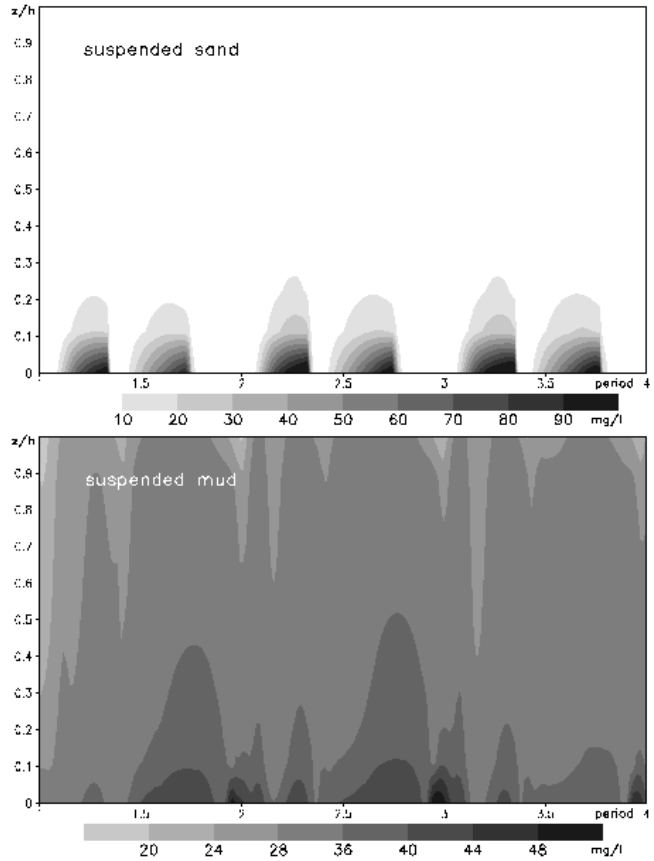

Fig. 3. Time versus depth diagrams for sand in suspension (top) and mud in suspension (bottom) at a position in the Otzumer Balje around spring tide.

Conclusions

The presented hydrodynamic model GETM together with the sediment transport model is a successful tool to theoretically investigate the sediment transport behaviour of the East Frisian Wadden Sea. Comparisons with measurements have shown the high accuracy of the hydrodynamic model. It is also capable of simulating the observed tidal asymmetries which have an important influence on the transport of the suspended sediment load. The sediment transport model takes all relevant processes into account, and the results show a consistent behaviour. The observed import of fine-grained material into the inlet during strong winds was reproduced by the model.

Although the hydrodynamic model has been tested many times in the last years and can be considered well calibrated, the sediment transport model has still to be adjusted by comparison with measurements. The bottom boundary condition, that both mud and sand are available for erosion throughout the whole model area, will have to be refined. A more detailed analysing of the interaction of the tidal asymmetry and the sediment transport will be a topic of future work.

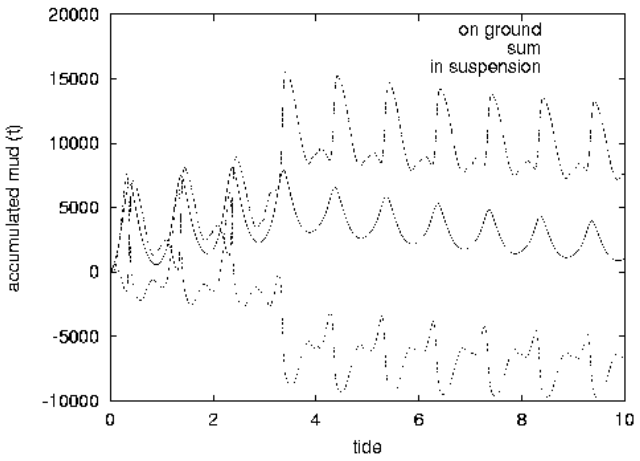

Fig. 5. Accumulated mud in the tidal basin of Spiekeroog with wind from north-west (6 Bft) for three tides. At the beginning of the fourth tide the wind was switched off. The topmost curve is the mud accumulated on the ground of the basin, the bottom curve is mud in suspension inside the basin, and the middle curve is the sum of both. The accumulated mud was set to zero at the beginning of the first tide.

References

ARAKAWA, A.& LAMB, V. R. (1977) Computational design of the basic dynamical processes of the UCLA general circulation model. Meth. Computat. Phys, **16**, 173-263.

BAGNOLD, R. A. (1966) An approach to the sediment transport problem from general physics. USGS Prof. Paper, **4421**, 37 pp.

BURCHARD, H. & BOLDING, K. (2002) GETM - a general estuarine transport model. Scientific documentation, No EUR 20253 EN, European Commission, printed in Italy, 157 pp.

KRONE, R. B. (1962) Flume studies of the transport of sediment in estuarial shoaling processes. Final Report, Hydraul. Eng. Lab., Sanitary Eng. Res. Lab., Univ. of California, Berkeley, 110 pp.

VAN LEUSSEN, W. (1988) Aggregation of particles, settling velocity of mud flocs, review. In: Dronkers, J. & van Leussen, W. (eds.), Physical processes in estuaries, Springer, Heidelberg, 347-404.

MEHTA, A. J. (1988) Laboratory studies on cohesive sediment deposition and erosion. In: Dronkers, J. & van Leussen, W. (eds.), Physical processes in estuaries, Springer, Heidelberg, 327-345.

PARTHENIADES, E. (1984) A fundamental framework for cohesive sediment deposits. In: Mehta, A. J. (ed.), Lecture notes on coastal and estuarine studies 14, Estuarine cohesive sediment dynamics, Springer, Heidelberg, 219-250.

PULS, W. & SÜNDERMANN, J. (1990) Simulation of suspended sediment dispersion in the North Sea. In: R.T. Cheng (ed.), Coastal and estuarine studies, **38**, Residual currents and long-term transport, Springer, New York.

RODI, W. (1980) Turbulence models and their application in hydraulics. Report Int. Assoc. for Hydraul. Res., Delft, Netherlands.

SANTAMARINA, C. P. & FLEMMING, B. W. (2000) Quantifying concentration and flux of suspended particulate matter through a tidal inlet of the East Frisian Wadden Sea by acoustic doppler current profiling. In: Flemming, B. W., Delafontaine, M. T. & Liebezeit, G. (eds.), Muddy coast dynamics and resource management, Elsevier, Amsterdam, 39-51.

STANEV, E., FLÖSER, G. & WOLFF, J.-O. (2003b) Dynamical control on water exchanges between tidal basins and the open ocean. A case study for the East Frisian Wadden Sea. Ocean Dynamics, PECS 2002 Special Issue.

STANEV, E., WOLFF, J.-O., BURCHARD, H., BOLDING, K. & FLÖSER, G. (2003a) On the circulation in the East Frisian Wadden Sea: Numerical modelling and data analysis Ocean Dynamics, **53**, 27-51.

[1]G. Brink-Spalink, [1]E. V. Stanev & [2]J.-O. Wolff, University of Oldenburg, ICBM, Carl-von-Ossietzky-Straße 9-11, D-26129 Oldenburg, Germany. [1]phone: +49 441 7984061. [2]phone: +49 441 7985343. fax: +49 441 7983404; e-mail: g.brink-spalink@icbm.de.